Anticancer drug oxaliplatin induces acute cooling-aggravated neuropathy via sodium channel subtype $Na_V1.6$-resurgent and persistent current

Ruth Sittl[a,1], Angelika Lampert[b,1], Tobias Huth[b], E. Theresa Schuy[b], Andrea S. Link[b], Johannes Fleckenstein[c], Christian Alzheimer[b], Peter Grafe[a], and Richard W. Carr[a,d,2]

[a]Institute of Physiology and [c]Department of Anesthesiology, Ludwig-Maximilians University, 80336 Munich, Germany; [b]Institute of Physiology and Pathophysiology, Friedrich-Alexander Universität Erlangen-Nürnberg, 91054 Erlangen, Germany; and [d]Department of Anesthesia and Intensive Care Medicine, Medical Faculty Mannheim, Heidelberg University, 68167 Mannheim, Germany

Edited by Richard W. Aldrich, University of Texas, Austin, TX, and approved March 8, 2012 (received for review November 2, 2011)

Infusion of the chemotherapeutic agent oxaliplatin leads to an acute and a chronic form of peripheral neuropathy. Acute oxaliplatin neuropathy is characterized by sensory paresthesias and muscle cramps that are notably exacerbated by cooling. Painful dysesthesias are rarely reported for acute oxaliplatin neuropathy, whereas a common symptom of chronic oxaliplatin neuropathy is pain. Here we examine the role of the sodium channel isoform $Na_V1.6$ in mediating the symptoms of acute oxaliplatin neuropathy. Compound and single-action potential recordings from human and mouse peripheral axons showed that cooling in the presence of oxaliplatin (30–100 μM; 90 min) induced bursts of action potentials in myelinated A, but not unmyelinated C-fibers. Whole-cell patch-clamp recordings from dissociated dorsal root ganglion (DRG) neurons revealed enhanced tetrodotoxin-sensitive resurgent and persistent current amplitudes in large, but not small, diameter DRG neurons when cooled (22 °C) in the presence of oxaliplatin. In DRG neurons and peripheral myelinated axons from *Scn8a*$^{med/med}$ mice, which lack functional $Na_V1.6$, no effect of oxaliplatin and cooling was observed. Oxaliplatin significantly slows the rate of fast inactivation at negative potentials in heterologously expressed m$Na_V1.6$r in ND7 cells, an effect consistent with prolonged Na_V open times and increased resurgent and persistent current in native DRG neurons. This finding suggests that $Na_V1.6$ plays a central role in mediating acute cooling-exacerbated symptoms following oxaliplatin, and that enhanced resurgent and persistent sodium currents may provide a general mechanistic basis for cold-aggravated symptoms of neuropathy.

chemotherapy | peripheral nerve | abnormal axonal excitability | repetitive action potential discharge

Clinical use of the highly effective chemotherapeutic oxaliplatin is compromised by an acute and a chronic form of peripheral neuropathy. Acutely, 85–90% of patients exhibit muscle fasciculations (1, 2), sensory paresthesias, and occasional dysesthesias (3), all triggered by mild cooling. Although chronic oxaliplatin-induced neuropathy has been recently linked to changes in the expression and sensitivity of transient receptor potential (TRP) channels TRPM8 and TRPA1 (4, 5), two-pore domain potassium channels (TREK1, TRAAK) and the hyperpolarization-activated channel HCN1 (6), the mechanism underlying acute oxaliplatin neuropathy remains unresolved. Several candidate mechanisms have been proposed including potassium channel blockade (7), calcium chelation (8), and alterations in voltage-gated sodium channel (Na_V) kinetics (9, 10), but none adequately account for motor and sensory symptoms nor their exacerbation by cooling.

Two tetrodotoxin (TTX)-resistant (TTX-r; $Na_V1.8$ and $Na_V1.9$) and five TTX-sensitive Na_v isoforms (TTX-s; $Na_V1.1$, -1.2, -1.3, -1.6, -1.7) are expressed in the peripheral nervous system. Na_vs generate the upstroke of the action potential (AP), but can also mediate persistent (I_{NaP}) and resurgent currents (I_{NaR}). I_{NaP} enhances excitability around firing threshold (11, 12) and mutations augmenting I_{NaP} have been linked to human forms of epilepsy ($Na_V1.1$) (13), arrhythmia ($Na_V1.5$) (14), paramyotonia congenita ($Na_v1.4$) (15, 16), and pain ($Na_v1.7$) (15, 17). I_{NaR} was first described in cerebellar Purkinje neurons and refers to a transient surge of inward sodium current occurring upon repolarization from a preceding period of strong depolarization (18). Because of its unorthodox activation profile, I_{NaR} is thought to promote burst discharge (11, 12).

Pain associated with paroxysmal extreme pain disorder (17) and muscle cramps experienced by paramyotonia patients (16) are often exacerbated or triggered by cooling, similar to the symptoms of acute oxaliplatin neuropathy. In the peripheral nervous system, large dorsal root ganglion neurons can generate I_{NaP} (19) and an $Na_V1.6$-mediated I_{NaR} (20). Combining single axon and patch-clamp recordings, the symptoms of acute oxaliplatin neuropathy appear to be because of a temperature-sensitive enhancement of I_{NaR} and I_{NaP}, with $Na_v1.6$ strongly implicated in mediating these effects.

Results

Burst Activity in Human Myelinated Axons During Cooling and Oxaliplatin. A direct effect on peripheral axons is likely to underlie acute oxaliplatin neuropathy. In vitro exposure of human myelinated axons to oxaliplatin (100 μM; 90 min) induced after-potentials in the A-fiber compound action potential (CAP) response to electrical stimulation at 30 °C (Fig. 1*A*, oxaliplatin, *Upper* traces). A-fiber after-potentials were typically discernible within 40 min and, consistent with cold-aggravated symptoms reported by patients, increased dramatically upon cooling by ~10 °C (Fig. 1*A*, oxaliplatin, *Lower* traces). Recordings of a C-fiber CAP from a human nerve fascicle that fortuitously contained very few functional A-fibers remained unaffected during cooling both before and after exposure to oxaliplatin (Fig. 1*B*).

$Na_V1.6$ Is Required for Cooling-Induced Bursts in Myelinated Axons Following Oxaliplatin. The restriction of oxaliplatin's effect to A-fibers prompted an examination of $Na_V1.6$, the predominant Na_V isoform at adult nodes of Ranvier (21). Similar to human fascicles, mouse sural nerve A-fiber CAP responses developed prominent after-potentials during cooling following oxaliplatin (Fig. 1*C*). After-potentials were completely absent in nerves from *Scn8a*$^{med/med}$ mice lacking functional $Na_V1.6$ (22) and approximately halved in

Author contributions: R.S., A.L., T.H., P.G., and R.W.C. designed research; R.S., A.L., T.H., E.T.S., A.S.L., J.F., P.G., and R.W.C. performed research; R.S., A.L., T.H., E.T.S., A.S.L., C.A., P.G., and R.W.C. analyzed data; and R.S., A.L., and R.W.C. wrote the paper.

The authors declare no conflict of interest.

This article is a PNAS Direct Submission.

[1]R.S. and A.L. contributed equally to this work.

[2]To whom correspondence should be addressed. E-mail: richard.carr@medma.uni-heidelberg.de.

This article contains supporting information online at www.pnas.org/lookup/suppl/doi:10.1073/pnas.1118058109/-/DCSupplemental.

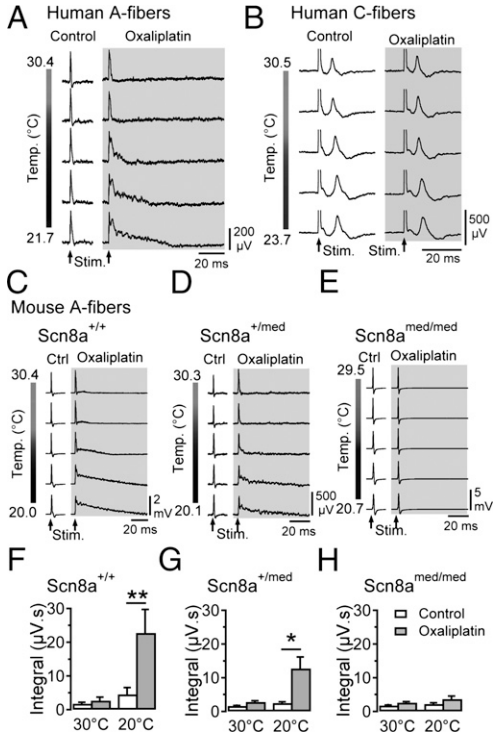

Fig. 1. Oxaliplatin and cooling-induced CAP-afterpotentials require $Na_V1.6$. Exposure of segments of human (*A* and *B*) and mouse (*C–E*) sural nerve to oxaliplatin (100 µM; ~90 min; gray) induces the emergence of after-potentials upon cooling following electrically evoked (Stim.) CAP responses in A-fibers (*A*, *C*, and *D*, $n = 8$ for human, and $n = 55$ for mouse nerve segments). The C-fiber CAP for a human nerve fascicle (*B*) that fortuitously contained very few functional A-fibers remains unaffected during cooling both before and after exposure to oxaliplatin. Cooling following oxaliplatin (gray) alters the shape of A-fiber responses from wild-type mice (*Scn8a*$^{+/+}$; *C*, $n = 8$ at 30 °C, 7 at 20 °C) and heterozygous (*Scn8a*$^{+/med}$; *D*, $n = 21$ at 30 °C, 16 at 20 °C), but not *Scn8a*$^{med/med}$ mice lacking $Na_V1.6$ (*E*, $n = 21$ at 30 °C, 16 at 20 °C). The magnitude of after-potential activity, quantified by integrating the voltage response following electrical stimulation (µV.s), is larger in recordings from wild-type mice than in those from *Scn8a*$^{+/med}$ mice (*F–H*). (*$P < 0.05$).

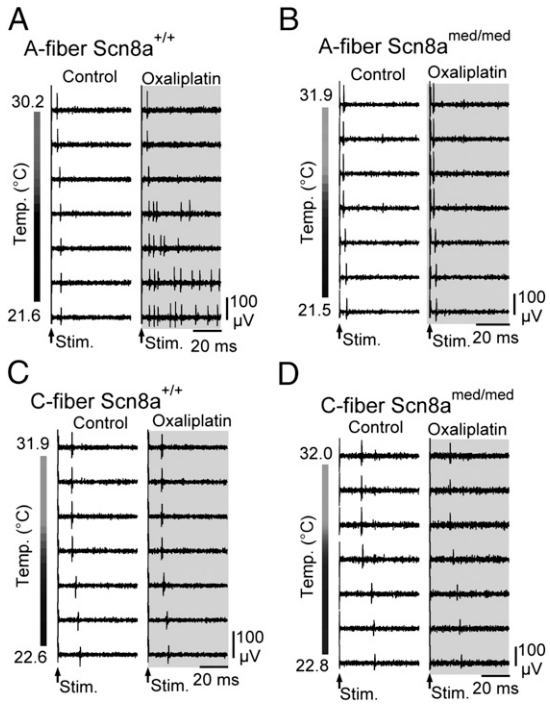

Fig. 2. Axonal effects of oxaliplatin and cooling are A-fiber specific and require $Na_V1.6$. Responses of individual A- and C-fibers from wild-type (*Scn8a*$^{+/+}$) and *Scn8a*$^{med/med}$ mice during cooling under control conditions and following exposure to oxaliplatin (100 µM; ~90 min; gray) show that cooling results in the induction of stimulus-evoked repetitive AP discharge selectively in single myelinated (*A*) but not unmyelinated (*C*) axons in wild-type mice. Single myelinated (*B*) and unmyelinated (*D*) axons from *Scn8a*$^{med/med}$ mice, lacking functional $Na_V1.6$, show no stimulus-evoked repetitive discharge upon cooling, highlighting the importance of $Na_V1.6$ for cooling-induced burst discharge.

nerve segments from heterozygous mice (Fig. 1 *D–H*). This finding implicates $Na_V1.6$ in the generation of stimulus-evoked burst discharge in A-fibers during cooling following oxaliplatin.

In single myelinated and unmyelinated axons, no change was observed in electrically evoked AP responses at physiological skin temperatures (~ 30–32 °C) neither in the presence nor absence of oxaliplatin (Fig. 2*A*, *Upper* traces). However, cooling to ~20 °C in oxaliplatin induced stimulus-evoked AP bursts in single myelinated axons (Fig. 2*A*, *Right*, *Lower* traces). This effect was absent in single A-fiber recordings from *Scn8a*$^{med/med}$ mice (Fig. 2*B*). Similar to CAP recordings from human C-fibers, the combination of cooling and oxaliplatin did not evoke burst responses in single murine C-fibers (Fig. 2 *C* and *D*, and Table S1).

Oxaliplatin Enhances Subthreshold Excitability in Myelinated Axons. To explore the possible excitatory role of I_{NaP} (23) in oxaliplatin-induced repetitive firing in axons, subthreshold electrical excitability was examined in mouse myelinated axons during cooling (25 ± 1 °C) before and after oxaliplatin (Fig. 3). Axonal excitability parameters sensitive to changes in membrane potential (24) were not altered by oxaliplatin (Table S2). However, the current amplitude required to evoke a 40% CAP response during a long-lasting depolarizing current pulse was found to be reduced by oxaliplatin. This result is evident in Fig. 3 *A* and *B* as an enhancement by oxaliplatin of the sustained excitability increase during a 100-ms depolarizing current pulse (Fig. 3*B*). Under control conditions, application of a depolarizing current results in an initial rapid increase in excitability (10–20 ms) that accommodates (90–100 ms, control) (Fig. 3*B*). Following oxaliplatin, the degree of threshold accommodation was less pronounced, indicative of persistent sodium current activation (Fig. 3 *B* and *E*, and Table S2). Consistent with the enhancement of a persistent sodium current, application of depolarizing current in the presence of oxaliplatin induced after-potentials in the A-fiber CAP response (Fig. 3*C*). In contrast, hyperpolarizing the axons suppressed after-potential activity (Fig. 3*D*).

Oxaliplatin and Cooling Enhance $Na_V1.6$-Mediated I_{NaR} in Large DRG Neurons. In addition to I_{NaP}, $Na_v1.6$ can also produce prominent I_{NaR}. Neurons with peripheral A-fibers have large somata (25) and, consequently, sodium currents were examined in large-diameter DRG neurons (40.6 ± 4.5 µm, 48.6 ± 18.6 pF, $n = 25$) using whole-cell patch-clamp. Under control conditions, TTX-s I_{NaR} was observed at 30 °C in DRG neurons from wild-type and, to a lesser extent, *Scn8a*$^{med/med}$ mice (Fig. 4 *A* and *B*). Exposure of wild-type and *Scn8a*$^{med/med}$ DRGs to oxaliplatin (30 µM) had little effect on peak I_{NaR} at 30 °C. However, at 22 °C oxaliplatin produced a large I_{NaR} in wild-type DRGs (Fig. 4*B*). A smaller I_{NaR} was also observed in DRGs from *Scn8a*$^{med/med}$ mice, but this proved to be secondary to a change in I_{NaP} (see below and Fig. 4*E*).

From the raw traces in Fig. 4 *A* and *C*, a noninactivating I_{NaP} is evident (Fig. 4*D*). To examine I_{NaR} in isolation, I_{NaP} determined between 400 and 475 ms was subtracted from peak I_{NaR}. This finding revealed a prominent I_{NaR} only in wild-type DRGs at 22 °C (Fig. 4*E*). This effect is not a result of variations in cell size, because I_{NaR} was still enhanced when expressed as current density (wild-type control 22.2 ± 3.4 pA/pF at 30 °C, 21.9 ± 4.9 at 22 °C pA/pF,

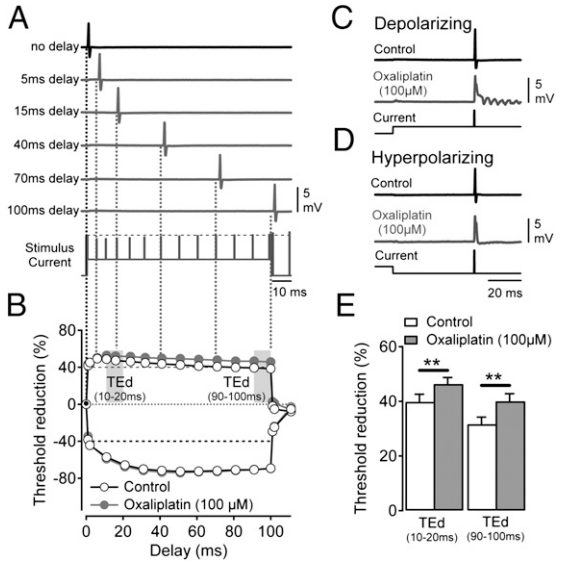

Fig. 3. Enhancement of depolarizing threshold electrotonus (TE) responses by oxaliplatin is positively correlated with repetitive after-activity in A-fibers. Changes in electrical threshold in response to polarizing current (TE) applied to myelinated axons. (*A*) The current amplitude required to evoke a 40% A-fiber CAP under control conditions (black uppermost trace and black vertical line in *A*, black marker in *B*) is used as a reference (horizontal broken black line in stimulus current trace). The current strength required to similarly evoke a 40% CAP response at discrete time points (delays) during application of polarizing current (*A*, stimulus current) was determined in sequential sweeps (gray traces). In the example illustrated in *A*, a conditioning depolarizing current of +40% of the control threshold current is applied over 100 ms. Individual sweeps show 40% CAP responses evoked at the indicated delay. (*B*) Representative examples of TE responses to ±40% polarizing current before (Control open markers) and after oxaliplatin (100 μM, ~90 min; filled gray markers) with the periods used for quantitative analysis is indicated in *E* (d, depolarizing; h, hyperpolarizing). (*C* and *D*) Representative examples of CAP responses to electrical stimulation during conditioning subthreshold depolarizing (*C*) and hyperpolarizing (*D*) current application (*Lowermost* trace) in the absence (Control, *Upper* trace) and presence of oxaliplatin (*Middle* traces, gray). (*E*) Pooled data for +40% depolarizing TE responses determined over 10–20 ms and 90–100 ms in the presence of vehicle (control) and oxaliplatin. Data were collected at a bath temperature of 25.5 ± 1 °C from nine wild-type mice aged 122–194 d and weighing between 24.4 and 34.0 g. (**$P < 0.01$).

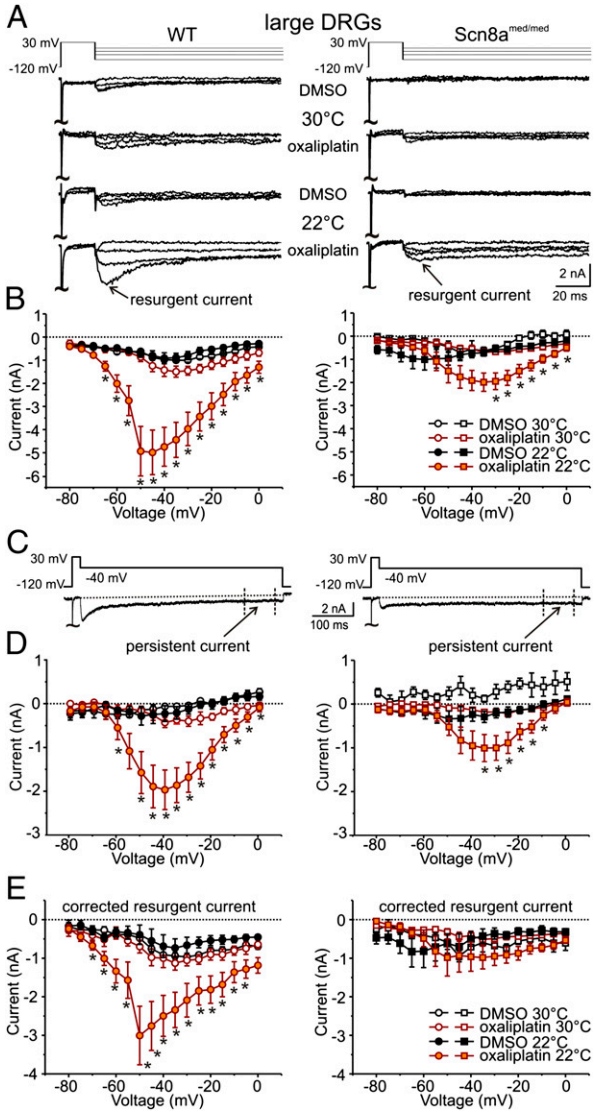

Fig. 4. Oxaliplatin and cooling enhance I_{NaR} and I_{NaP} TTX-s Na_V currents in large-diameter DRG neurons. (*A*) Representative current traces in response to voltage commands to −75, −45, −25, and −5 mV (*Upper* lane) from large-diameter (40.6 ± 4.5 μm, $n = 25$) DRG neurons from wild-type (WT, *Left*) and *Scn8a*$^{med/med}$ mice (*Right*) at 30 °C and 22 °C after incubation with oxaliplatin (30 μM; ~90 min). (*B*) Peak I_{NaR} as a function of voltage for recordings at 30 °C [open symbols: WT $n = 5;5$ and *Scn8a*$^{med/med}$: $n = 4;6$ (DMSO; oxaliplatin)] and 22 °C (filled symbols, WT: $n = 10;11$, *Scn8a*$^{med/med}$: $n = 6;8$) from DRG neurons incubated with vehicle (1% vol/vol DMSO) or oxaliplatin. (*C*) Representative voltage command (*Upper*) and current (*Lower*) traces indicating the period over which the I_{NaP} component was determined (400–475 ms). (*D*) I_{NaP} shown as a function of voltage for recordings at 30 °C (open symbols, WT $n = 5;5$ and *Scn8a*$^{med/med}$ $n = 8;11$ for DMSO; oxaliplatin) and 22 °C (filled symbols, WT: $n = 10;11$, *Scn8a*$^{med/med}$: $n = 6;8$) from large-diameter DRG neurons (WT *Left*, *Scn8a*$^{med/med}$ *Right*) after incubation with vehicle (black) or oxaliplatin (orange). (*E*) Corrected I_{NaR} amplitude as a function of voltage for recordings at 30 °C (open) and 22 °C (filled) from large-diameter DRG neurons (WT *Left*, *Scn8a*$^{med/med}$ *Right*) after incubation with vehicle (black) or oxaliplatin (orange). I_{NaR} was corrected for each individual trace by subtracting the I_{NaP} component (*D*) from the peak I_{NaR} (*B*). Mice ranging in age from P14–25 were used. (*$P < 0.05$, **$P < 0.01$).

$n = 5;8$, $P = 0.56$; oxaliplatin, 29.6 ± 3.8 pA/pF at 30 °C, 57.3 ± 10.6 pA/pF at 22 °C, $n = 5;11$, $P < 0.05$).

Consistent with the observations for single C-fibers in peripheral nerve (Fig. 2*C*), TTX-s I_{NaR} was not observed in small (20.3 ± 2.7 μm) DRGs under control conditions nor following oxaliplatin at 22 °C ($n = 12$) (Fig. S1).

Oxaliplatin and Cooling Affect I_{NaP} in Large DRG Neurons. The combination of oxaliplatin and cooling enhanced the magnitude of I_{NaP} in large-diameter DRG neurons from both wild-type and *Scn8a*$^{med/med}$ mice (Fig. 4*D*). The increase in I_{NaP} seen in wild-type neurons spanned a greater voltage range and was larger in amplitude than that from *Scn8a*$^{med/med}$ DRGs. For DRG neurons from *Scn8a*$^{med/med}$ mice, the increase in I_{NaP} under combined oxaliplatin and cooling dominated and accounts for the apparent increase in I_{NaR} (Fig. 4 *B* and *E*, *Right*).

To address the possibility that the preceding strong depolarization required to evoke I_{NaR} might have influenced I_{NaP}, current responses to a standard depolarizing step protocol were also examined (Fig. S2*A*) and, indeed, using this protocol a comparable increase in I_{NaP} was observed in DRGs from wild-type and *Scn8a*$^{med/med}$ mice following oxaliplatin and cooling (Fig. S2).

Oxaliplatin Slows Fast Inactivation in Heterologously Expressed $Na_V1.6$. In contrast to oxaliplatin's pronounced effects on I_{NaR} and I_{NaP} in DRG neurons at low temperatures, TTX-s Na_V activation and steady-state fast inactivation were not affected (n = 4–10) (Fig. S3 and Table S3). Because several Na_v isoforms

contribute to sodium currents in isolated DRG neurons, the effect of oxaliplatin on $Na_v1.6$ was examined in isolation in neuron-derived ND7/23 cells transfected with murine $Na_V1.6r$ and auxiliary β4-subunit. Consistent with previous reports (26), heterologous coexpression of $mNa_V1.6r$ and β4 failed to yield appreciable I_{NaR} (Fig. S4). Oxaliplatin shifted steady-state fast inactivation for $mNa_V1.6r$ in the depolarizing direction (V_{half} control: -65.9 ± 0.8 mV; oxaliplatin: -61.7 ± 0.7 mV; $P < 0.001$) but was without effect on the voltage-dependence of activation (Fig. S5). However, oxaliplatin (30 μM) affected the rate of fast inactivation in a voltage-dependent manner, considerably slowing inactivation at negative membrane potentials (Fig. 5*C*).

A voltage-dependent slowing of fast inactivation by oxaliplatin could lead to an enhanced I_{NaR} by increasing Na_V open time at negative membrane potentials following expulsion of the blocking particle (Fig. 5*D*, arrow 2). This possibility was examined formally using numerical simulations in an established model of I_{NaR} in a cerebellar Purkinje neuron (27, 28). The model was adjusted initially (see *Materials and Methods*) to emulate the experimentally determined kinetics of I_{NaR} in DRG neurons (Fig. 5*E*). Selective slowing of the inactivation rate constant (Oon) resulted in an enhanced resurgent sodium current and the induction of a persistent current component (Fig. 5*E* and *Discussion*) comparable to that observed in DRG neurons exposed to oxaliplatin at 22 °C (Fig. 5*A*).

Discussion

Acute cooling-aggravated neuropathy affects the overwhelming majority (>80%) of patients receiving intravenous oxaliplatin (1, 2). Using electrophysiological recordings from human and mouse peripheral nerve, it has been possible to show that these cooling-aggravated symptoms can be attributed to the induction of aberrant burst discharges in peripheral myelinated axons, with C-fibers remaining notably unaffected. Oxaliplatin slows the time course of fast inactivation in cell-expressed $Na_v1.6$ and, in combination with cooling, this may favor a specific enhancement of $Na_v1.6$-mediated I_{NaR} and I_{NaP} in large-diameter DRG neurons. The enhanced I_{NaR} is further thought to underlie burst-firing in peripheral sensory and motor myelinated axons expressing $Na_v1.6$, and thus the symptoms of acute oxaliplatin neuropathy.

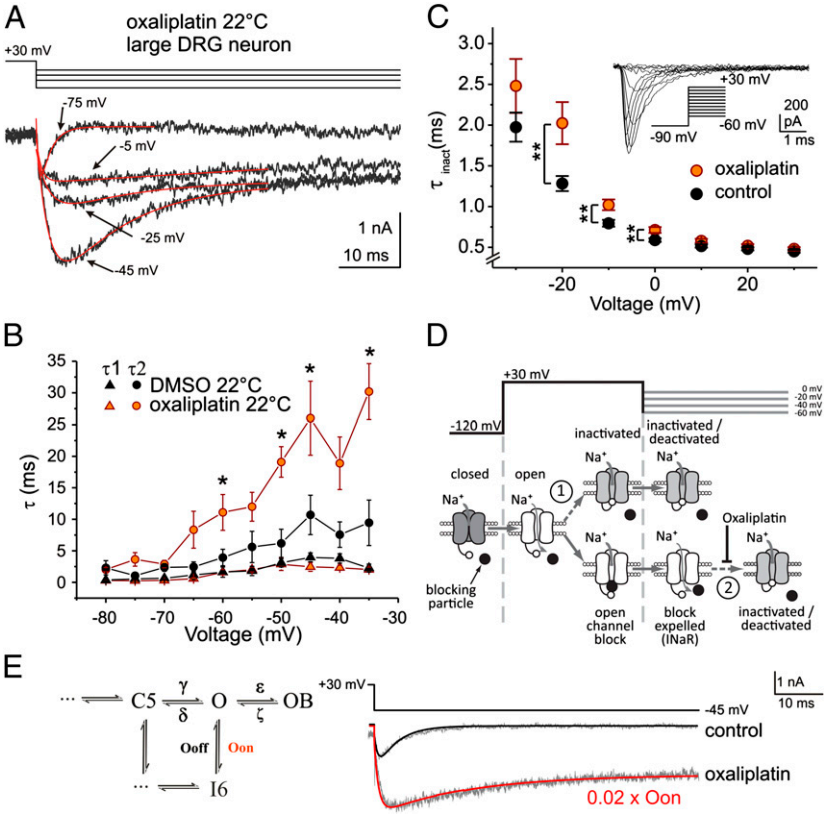

Fig. 5. Oxaliplatin slows the rate of decay of resurgent current in large DRG neurons and slows fast inactivation in $mNa_V1.6r$ in ND7 cells. (*A*) Representative current recordings (*Lower*) from a DRG neuron in response to the voltage protocol (*Upper*). Current traces were fitted with a double-exponential function. (*B*) Rise (τ1, triangles) and decay (τ2, circles) time constants for resurgent current evoked by the protocol in *A* as a function of voltage at 22 °C (DMSO: black symbols, $n = 7$; oxaliplatin 30 μM: orange symbols, $n = 10$). (*C*) Time constant of mNaV1.6r current inactivation as a function of voltage. mNaV1.6r was expressed with β4 in ND7 cells and currents were evoked by voltage steps from −90 mV to potentials ranging from −60 to +30 mV (control: black symbols, $n = 29$; oxaliplatin 30 μM: orange symbols, $n = 28$). (*Inset*) Depiction of voltage commands (*Lower Right*) and current recordings. All recordings were performed at room temperature (~22 °C). (*D*) Simplified Na_V gating schematic indicating state transitions during the voltage protocol used to evoke resurgent current in DRG neurons. At −120 mV, Na_Vs are closed (dark gray) and open (white) upon depolarization to +30 mV. At positive potentials, open channels may either inactivate (arrow 1, *Upper*) or, if an appropriate blocking particle (black circle) is present, block in the open configuration (*Lower*). Upon partial repolarization to voltages between 0 and −60 mV, the blocking particle is expelled by permeating Na^+ generating a resurgent current (I_{NaR}). Resurgent current is terminated either by fast inactivation (arrow 2) or deactivation (not shown). In mNav1.6r, oxaliplatin slowed fast inactivation voltage dependently at potentials in the range of I_{NaR} (*C*). (*E*) Comparison of DRG current recordings (gray) and mathematical simulations (black and red). To mimic the empirical slowing of fast inactivation by oxaliplatin (*Lower* gray trace), the rate constant (Oon) for the state transition from open (O) to inactivated (I6) was reduced to 2% of its original value (0.02 × Oon), resulting in an increase in the magnitude of simulated resurgent current and the emergence of a persistent current component. (*$P < 0.05$, **$P < 0.01$).

$Na_V1.6$ is the predominant nodal sodium channel expressed in peripheral motor and sensory myelinated axons (21, 29), providing the primary current for AP propagation (30). Because native $Na_v1.6$ can readily generate I_{NaR} (20, 31) and I_{NaP} (31), an enhancement of both current components could readily account for aberrant axonal burst-firing following oxaliplatin and cooling.

I_{NaR} is thought to be generated through dislodgment of an open-channel blocking particle from the Na_V permeation pathway upon repolarization (32) (Fig. 5*D*). The cytoplasmic tail of the β4-subunit has been postulated to serve as an endogenous blocking particle (33, 34) and β4 is present in both spinal motoneurons and DRG neurons (35). Binding of the blocking particle is favored when the channel is open and inactivation is slowed. Accordingly, toxins, such as β-pompilidotoxin, that slow fast inactivation promote I_{NaR} (36). Similarly, oxaliplatin slowed fast inactivation in $Na_v1.6$, but significantly only at potentials ≤ 0 mV (Fig. 5*C*). By delaying inactivation, oxaliplatin could enhance I_{NaR} by increasing $Na_V1.6$ open probability (Fig. 5*D*, arrow 2). Experimentally, temperature is shown to be a crucial cofactor for enhanced I_{NaR} (Fig. 4*B*). Cooling would be expected to slow inactivation in a voltage-independent manner, increasing both the likelihood and thus number of channels in the open-channel block configuration (Fig. 5*D*, arrow 1), as well as prolonging channel-open times following dislodgment of the open-channel blocker (Fig. 5*D*, arrow 2). This finding is particularly relevant for myelinated axons in which inactivation (Q_{10}~2.9) of nodal sodium current is more prominently slowed by cooling than activation (Q_{10}~2.2) (37).

In addition to slowing fast inactivation, it is possible that oxaliplatin and cooling may further destabilize inactivation by affecting the binding affinity and kinetics of the blocking particle itself. This possibility, however, remains speculative with the intricate nature of the open-channel blocking process underlying I_{NaR} not yet fully resolved.

An enhancement of I_{NaP} was observed in large DRG neurons from wild-type and, to a lesser extent, *Scn8a*$^{med/med}$ mice, indicating that Na_V isoforms in addition to $Na_V1.6$ are likely to be involved. $Na_v1.2$ and $Na_v1.1$ (38) have been previously shown to contribute to I_{NaP} in DRG neurons (39) and, although a distinct I_{NaP} component has not been reported for Nav1.7 and Nav1.3, it is also possible that these two sodium channel subtypes could contribute to the enhancement of I_{NaP}.

I_{NaP} has been proposed to result from occasional failures of regular fast inactivation (40). Oxaliplatin's impairment of fast inactivation in $Na_V1.6$ (Fig. 5*C*) is likely to impact on I_{NaP}, in particular during cooling, which slows overall gating kinetics. In axons, I_{NaP} can be assessed using depolarizing threshold electrotonus responses and, despite studies in oxaliplatin-treated patients at 32 °C showing little change (41), the ability to cool nerve segments in vitro revealed a facilitation of I_{NaP} by oxaliplatin in peripheral myelinated axons in vitro (Fig. 3 *B* and *E*).

The increased excitability of A-fibers, and not C-fibers, together with the enhancement of I_{NaR} seen during cooling in combination with oxaliplatin, provides a general mechanistic basis for neuropathologies triggered or enhanced by cold, such as paroxysmal extreme pain disorder (17) and neuropathic pain following traumatic injury (42) or amputation (43).

Materials and Methods

Experiments on Human and Mouse Nerve. Approval for the experimental use of human nerve (from five male patients, 57 ± 9 y of age) was granted by the Ethics Committee of the Medical Faculty of the University of Munich (348/00). Patients gave their written consent before surgery. The diagnosis precipitating biopsy or amputation was typically polyneuropathy of unknown etiology or peripheral vascular disease.

Scn8a^{med} mice (kindly provided by Heinz Beck, University of Bonn Medical Center, Bonn, Germany) were used in accordance with ethical guidelines stipulated by German federal law (Tierschutzgesetz §1 and §4 Abs. 3). Since $Na_v1.6$ mice die around postnatal day (P) 20, mice ranging from P10–P30 were used [killed by enflurane (P10–20) or carbon dioxide (>P20)]. I_{NaP} and I_{NaR} have been reported not to change after P14 in mice (44).

CAP recordings. Segments of Nervus suralis (15–25 mm) were isolated, desheathed, and mounted between suction electrodes in an organ bath. The perfusing solution (117 mM NaCl, 3.6 mM KCl, 2.5 mM $CaCl_2$, 1.2 mM $MgCl_2$, 1.2 mM NaH_2PO_4, 25 mM $NaHCO_3$, 11 mM D-glucose, bubbled with 95% O_2 – 5% CO_2 to pH 7.4) was temperature-controlled. CAPs and single APs were recorded extracellularly in response to constant current stimulation (0.1 ms, A395; World Precision Instruments) at 0.1 Hz and analyzed with IgorPro (Wavemetrics).

Single-fiber recordings. An isolated section of mouse skin with its innervating Nervus saphenous was perfused with solution (see above) at 32.0 ± 0.5 °C. Single APs were distinguished by consistency of spike shape and response latency. Signals were filtered (<5 kHz), amplified (Axopatch 200A; Axon), digitized (μ1401; Cambridge Electronic Design), and only a single unit per skin preparation was used.

After a control period (~30 min) at 30–32 °C comprising a 5-min period of cooling (to 20 °C), oxaliplatin (10–100 μM) was added for 120 min, and at 90 min a second 5-min period of cooling was applied.

Excitability testing. The electrical excitability of myelinated axons was determined by tracking the stimulus current intensity required to maintain an A-fiber CAP of 40% amplitude during application of subthreshold polarizing currents or conditioning stimuli. Excitability parameters were determined in QTRAC (Hugh Bostock, University of London, United Kingdom) using the TRONDXS4 protocol with a 0.5-ms test pulse at bath temperatures between 24.5 °C and 26.5 °C.

Whole-Cell Patch-Clamp Recordings. Cultured DRG neurons (45) were incubated in either oxaliplatin (30 μM) or vehicle (DMSO 1% vol/vol) for 98 min ± 16 min. Neuron diameter was estimated from a digital image. Whole-cell voltage-clamp recordings (EPC-10USB; HEKA) were performed 1 d after plating using glass electrodes (1–1.5 MΩ) containing: 140 mM CsF, 10 mM NaCl, 1 mM EGTA, 10 mM Hepes (pH 7.38, CsOH). The external solution was tempered with an in-line heater (Warner Instruments) and contained: 140 mM NaCl, 3 mM KCl, 1 mM $MgCl_2$, 1 mM $CaCl_2$, 5 mM D-glucose, 10 mM Hepes, 20 mM TEA-Cl, 0.1 mM $CdCl_2$ (pH 7.38, NaOH). For I-V curves and steady-state fast inactivation, sodium was reduced to 10 mM externally (substituted with choline) and to 2 mM internally. Series resistance was compensated to 2.7 ± 0.4 MΩ. P/4 leak correction was applied. TTX-s currents were determined by subtraction following TTX (0.5–1 μM).

Voltage protocols (0.2 Hz) were applied from either −120 mV (I_{NaR} and I_{NaP}) or −90 mV (I-V and fast inactivation). For protocols, see Figs. 4 and 5. Peak I_{NaR} was determined during the first 50 ms following step back; I_{NaP} refers to the mean current over the 400- to 475-ms period. Half-maximum voltage (V_{half}) and slope (*k*) of activation and inactivation were determined from Boltzmann fits.

A double-exponential fit was used to determine rise (τ1) and decay (τ2) time constants from resurgent current traces (Fig. 5*A*). The fit was restricted in the time domain to a period either 20 ms (−80 mV and −70 mV) or 40 ms (potentials > −70 mV) after repolarization from the prepulse.

$mNa_V1.6$ (46) was mutated to the TTX-r variant ($mNa_V1.6r$, Y371S, QuikChange II XL; Agilent Technologies) and cotransfected with mβ4-GFP (47) into neuroblastoma ND7 cells. Whole-cell patch-clamp recordings (pClamp, Digidata 1322A; Axon) were performed at room temperature using the following solutions: bath: 145 mM NaCl, 4 mM KCl, 2 mM $CaCl_2$, 2 mM $MgCl_2$, 10 mM D-Glucose, 10 mM Hepes, 10 mM TEA, 0.001 mM TTX, pH 7.4 (NaOH); pipette: 125 mM CsCl, 5 mM NaCl, 2 mM Mg_2ATP, 10 mM Hepes, 5 mM EGTA (pH 7.2, CsOH). Cells were incubated with oxaliplatin (30 μM, >30 min). Fast inactivation time constants were determined from activation protocols using single exponential fits over the 4.45-ms period following the peak current.

NEURON Simulation. Simulations were performed in NEURON (48) for Na_V currents in a cerebellar Purkinje neuron incorporating I_{NaR} (27, 28) and comprising closed (C), open (O), open-channel blocked (OB), and inactivated (I) states. Initial adjustment to model parameters ε (from 1.75 to 0.02) and Ooff (from 0.005 to 0.001) were made to emulate the empirical control trace (Fig. 5*E*, gray traces).

Chemicals. Drugs were added to external solutions on the day of each experiment from stock solutions; oxaliplatin (Sigma-Aldrich) was solved in DMSO and TTX in distilled water. DMSO (0.1–1% vol/vol) applied alone to each of the preparations had no detectable effect.

Statistics. Data are presented as mean ± SEM for comparisons between groups and mean ± SD for population descriptors. A two-way ANOVA with post hoc Scheffé or Student *t* test were used for statistical comparisons.

ACKNOWLEDGMENTS. We thank M. Schmelz and A. M. Rush for comments on the manuscript, and A. Wirth-Hücking and I. Plonner for technical assistance. This work was supported by grants from the Deutsche Forschungsgemeinschaft (DFG) GR801/3-1 (to P.G.); LA2740/2-1 (to A.L.); CA853/1-2 (to R.C.), and the Kompetenzzentrum Schmerz Baden-Württemberg.

1. Lehky TJ, Leonard GD, Wilson RH, Grem JL, Floeter MK (2004) Oxaliplatin-induced neurotoxicity: Acute hyperexcitability and chronic neuropathy. *Muscle Nerve* 29: 387–392.
2. Hill A, et al. (2010) Detecting acute neurotoxicity during platinum chemotherapy by neurophysiological assessment of motor nerve hyperexcitability. *BMC Cancer* 10:451.
3. Raymond E, Chaney SG, Taamma A, Cvitkovic E (1998) Oxaliplatin: A review of preclinical and clinical studies. *Ann Oncol* 9:1053–1071.
4. Gauchan P, Andoh T, Kato A, Kuraishi Y (2009) Involvement of increased expression of transient receptor potential melastatin 8 in oxaliplatin-induced cold allodynia in mice. *Neurosci Lett* 458:93–95.
5. Nassini R, et al. (2011) Oxaliplatin elicits mechanical and cold allodynia in rodents via TRPA1 receptor stimulation. *Pain* 152:1621–1631.
6. Descoeur J, et al. (2011) Oxaliplatin-induced cold hypersensitivity is due to remodelling of ion channel expression in nociceptors. *EMBO Mol Med* 3:266–278.
7. Kagiava A, Tsingotjidou A, Emmanouilides C, Theophilidis G (2008) The effects of oxaliplatin, an anticancer drug, on potassium channels of the peripheral myelinated nerve fibres of the adult rat. *Neurotoxicology* 29:1100–1106.
8. Grolleau F, et al. (2001) A possible explanation for a neurotoxic effect of the anticancer agent oxaliplatin on neuronal voltage-gated sodium channels. *J Neurophysiol* 85:2293–2297.
9. Adelsberger H, et al. (2000) The chemotherapeutic oxaliplatin alters voltage-gated Na(+) channel kinetics on rat sensory neurons. *Eur J Pharmacol* 406:25–32.
10. Webster RG, Brain KL, Wilson RH, Grem JL, Vincent A (2005) Oxaliplatin induces hyperexcitability at motor and autonomic neuromuscular junctions through effects on voltage-gated sodium channels. *Br J Pharmacol* 146:1027–1039.
11. Enomoto A, Han JM, Hsiao C-F, Wu N, Chandler SH (2006) Participation of sodium currents in burst generation and control of membrane excitability in mesencephalic trigeminal neurons. *J Neurosci* 26:3412–3422.
12. Do MT, Bean BP (2003) Subthreshold sodium currents and pacemaking of subthalamic neurons: Modulation by slow inactivation. *Neuron* 39:109–120.
13. Kahlig KM, Misra SN, George AL, Jr. (2006) Impaired inactivation gate stabilization predicts increased persistent current for an epilepsy-associated SCN1A mutation. *J Neurosci* 26:10958–10966.
14. Deschênes I, et al. (2000) Electrophysiological characterization of SCN5A mutations causing long QT (E1784K) and Brugada (R1512W and R1432G) syndromes. *Cardiovasc Res* 46:55–65.
15. Jarecki BW, Piekarz AD, Jackson JO, 2nd, Cummins TR (2010) Human voltage-gated sodium channel mutations that cause inherited neuronal and muscle channelopathies increase resurgent sodium currents. *J Clin Invest* 120:369–378.
16. Ptácek LJ, et al. (1992) Mutations in an S4 segment of the adult skeletal muscle sodium channel cause paramyotonia congenita. *Neuron* 8:891–897.
17. Fertleman CR, et al. (2006) SCN9A mutations in paroxysmal extreme pain disorder: Allelic variants underlie distinct channel defects and phenotypes. *Neuron* 52:767–774.
18. Raman IM, Bean BP (1997) Resurgent sodium current and action potential formation in dissociated cerebellar Purkinje neurons. *J Neurosci* 17:4517–4526.
19. Baker MD, Bostock H (1997) Low-threshold, persistent sodium current in rat large dorsal root ganglion neurons in culture. *J Neurophysiol* 77:1503–1513.
20. Cummins TR, Dib-Hajj SD, Herzog RI, Waxman SG (2005) Nav1.6 channels generate resurgent sodium currents in spinal sensory neurons. *FEBS Lett* 579:2166–2170.
21. Caldwell JH, Schaller KL, Lasher RS, Peles E, Levinson SR (2000) Sodium channel Na(v) 1.6 is localized at nodes of ranvier, dendrites, and synapses. *Proc Natl Acad Sci USA* 97: 5616–5620.
22. Kohrman DC, Harris JB, Meisler MH (1996) Mutation detection in the med and medJ alleles of the sodium channel Scn8a. Unusual splicing due to a minor class AT-AC intron. *J Biol Chem* 271:17576–17581.
23. Sittl R, Carr RW, Grafe P (2011) Sustained increase in the excitability of myelinated peripheral axons to depolarizing current is mediated by Nav1.6. *Neurosci Lett* 492: 129–133.
24. Bostock H, Cikurel K, Burke D (1998) Threshold tracking techniques in the study of human peripheral nerve. *Muscle Nerve* 21:137–158.
25. Lawson SN (2002) Phenotype and function of somatic primary afferent nociceptive neurones with C-, Adelta- or Aalpha/beta-fibres. *Exp Physiol* 87:239–244.
26. Aman TK, et al. (2009) Regulation of persistent Na current by interactions between beta subunits of voltage-gated Na channels. *J Neurosci* 29:2027–2042.
27. Khaliq ZM, Gouwens NW, Raman IM (2003) The contribution of resurgent sodium current to high-frequency firing in Purkinje neurons: An experimental and modeling study. *J Neurosci* 23:4899–4912.
28. Huth T, Rittger A, Saftig P, Alzheimer C (2011) β-Site APP-cleaving enzyme 1 (BACE1) cleaves cerebellar Na+ channel β4-subunit and promotes Purkinje cell firing by slowing the decay of resurgent Na+ current. *Pflugers Arch* 461:355–371.
29. Boiko T, et al. (2001) Compact myelin dictates the differential targeting of two sodium channel isoforms in the same axon. *Neuron* 30:91–104.
30. Wilson MJ, et al. (2011) μ-Conotoxins that differentially block sodium channels NaV1.1 through 1.8 identify those responsible for action potentials in sciatic nerve. *Proc Natl Acad Sci USA* 108:10302–10307.
31. Raman IM, Sprunger LK, Meisler MH, Bean BP (1997) Altered subthreshold sodium currents and disrupted firing patterns in Purkinje neurons of Scn8a mutant mice. *Neuron* 19:881–891.
32. Aman TK, Raman IM (2010) Inwardly permeating Na ions generate the voltage dependence of resurgent Na current in cerebellar Purkinje neurons. *J Neurosci* 30: 5629–5634.
33. Bant JS, Raman IM (2010) Control of transient, resurgent, and persistent current by open-channel block by Na channel beta4 in cultured cerebellar granule neurons. *Proc Natl Acad Sci USA* 107:12357–12362.
34. Grieco TM, Malhotra JD, Chen C, Isom LL, Raman IM (2005) Open-channel block by the cytoplasmic tail of sodium channel beta4 as a mechanism for resurgent sodium current. *Neuron* 45:233–244.
35. Yu FH, et al. (2003) Sodium channel beta4, a new disulfide-linked auxiliary subunit with similarity to beta2. *J Neurosci* 23:7577–7585.
36. Grieco TM, Raman IM (2004) Production of resurgent current in NaV1.6-null Purkinje neurons by slowing sodium channel inactivation with beta-pompilidotoxin. *J Neurosci* 24:35–42.
37. Schwarz JR, Eikhof G (1987) Na currents and action potentials in rat myelinated nerve fibres at 20 and 37 degrees C. *Pflugers Arch* 409:569–577.
38. Kalume F, Yu FH, Westenbroek RE, Scheuer T, Catterall WA (2007) Reduced sodium current in Purkinje neurons from Nav1.1 mutant mice: implications for ataxia in severe myoclonic epilepsy in infancy. *J Neurosci* 27:11065–11074.
39. Rush AM, Cummins TR, Waxman SG (2007) Multiple sodium channels and their roles in electrogenesis within dorsal root ganglion neurons. *J Physiol* 579:1–14.
40. Alzheimer C, Schwindt PC, Crill WE (1993) Modal gating of Na+ channels as a mechanism of persistent Na+ current in pyramidal neurons from rat and cat sensorimotor cortex. *J Neurosci* 13:660–673.
41. Park SB, et al. (2009) Oxaliplatin-induced neurotoxicity: Changes in axonal excitability precede development of neuropathy. *Brain* 132:2712–2723.
42. Collins ED, Novak CB, Mackinnon SE, Weisenborn SA (1996) Long-term follow-up evaluation of cold sensitivity following nerve injury. *J Hand Surg Am* 21:1078–1085.
43. Carlsson IK, Rosén B, Dahlin LB (2010) Self-reported cold sensitivity in normal subjects and in patients with traumatic hand injuries or hand-arm vibration syndrome. *BMC Musculoskelet Disord* 11:89.
44. Fry M (2006) Developmental expression of Na^+ currents in mouse Purkinje neurons. *Eur J Neurosci* 24:2557–2566.
45. Cummins TR, Rush AM, Estacion M, Dib-Hajj SD, Waxman SG (2009) Voltage-clamp and current-clamp recordings from mammalian DRG neurons. *Nat Protoc* 4: 1103–1112.
46. Leipold E, Hansel A, Borges A, Heinemann SH (2006) Subtype specificity of scorpion beta-toxin Tz1 interaction with voltage-gated sodium channels is determined by the pore loop of domain 3. *Mol Pharmacol* 70:340–347.
47. Huth T, et al. (2009) Non-proteolytic effect of beta-site APP-cleaving enzyme 1 (BACE1) on sodium channel function. *Neurobiol Dis* 33:282–289.
48. Hines ML, Carnevale NT (1997) The NEURON simulation environment. *Neural Comput* 9:1179–1209.